Supplementary Information

Efficient Oxidative Upcycling of Waste Polyolefins into Functional Carboxylic Acid Additives over Non-Noble-Metal Catalysts

Yi Hao,†[a] Kaili Wang,†[a] Rongrong Jia,[b] Ping Cheng,[c] Xin Feng,[a] Li Li,[d] Guanna Li, *[e] Liyi Shi *[a,f] and Lei Huang *[a]

[a]Research Center of Nano Science and Technology, College of Sciences, Shanghai University, Shanghai 200444, China.

[b]Department of Physics, College of Sciences, Shanghai University, Shanghai 200444, China.

[c]School of Environmental and Chemical Engineering, Shanghai University, Shanghai 200444, China.

[d]Engineering Research Center of Food Thermal-Processing Technology, College of Food Science and Technology, Shanghai Ocean University, Shanghai 201306, China.

[e]Biobased Chemistry and Technology, Wageningen University, Bornse Weilanden 9, 6708WG Wageningen, The Netherlands.

[f]Emerging Industries Institute, Shanghai University, Jiaxing, Zhejiang 314006, China.

†These authors contributed equally to this work.

*Corresponding author.

E-mail: leihuang@shu.edu.cn (L. Huang); shiliyi@shu.edu.cn (L. Shi); guanna.li@wur.nl (G. Li)

I. Supplementary Methods

Materials

Commercially available chemicals and solvents were used without further purification unless otherwise indicated. ZSM-5 (Si/Al = 38) was purchased from Xianfeng Nano Co., Ltd. (Jiangsu, China), and all other catalysts were obtained from suppliers listed on the Guidechem platform (http://www.guidechem.com). Anhydrous ethanol (EtOH, AR) and methanol (MeOH, AR) were obtained from Sinopharm Chemical Reagent Co., Ltd. Boron trifluoride–MeOH (50 wt%) was purchased from Shanghai Titan Scientific Co., Ltd. The 0.05 mol KOH–EtOH standard titration solution was obtained from Ronpharm Technology (Shanghai) Co., Ltd. Ultrapure water from the Milli-Q Reference system was used in this work. *S. aureus* (ATCC 6538) and *E. coli* (ATCC 25922) were obtained from Shanghai Luwei Technology Co., Ltd. (Shanghai, China).

PE/PP plastics characterization

High temperature gel permeation chromatography (GPC) analysis of all feedstocks was obtained by an Agilent Technologies PL-GPC-220 high temperature chromatograph, with trichlorobenzene as solvent and a flow rate of 1.00 mL/min.

Catalyst characterization

Thermogravimetric analysis (TG) of both fresh and used catalysts was conducted using the HITACHI STA200 instrument (TA Instruments) under a nitrogen gas flow, with a temperature range from 30 °C to 800 °C and a heating rate of 20 °C/min. The Brunauer-Emmett-Teller (BET) specific surface area was measured using a Micromeritics ASAP 2460 instrument. X-ray diffraction (XRD) patterns were obtained utilizing a Bruker D2 machine equipped with a Cu Kα source operating at 40 kV and 40 mA. Transmission electron microscopy (TEM) images were captured using a field emission high-resolution transmission electron microscope (FEI Tecnai G2 F20, Thermo Fisher) at an acceleration voltage of 200 kV. The X-ray photoelectron spectra (XPS) were recorded using a Thermo Scientific K-Alpha spectrometer using Al K Alpha radiation source. The binding energy was calibrated by the C 1s peak at 284.8 eV.

Catalytic oxidative upcycling of lab-grade PE/PP mixture

The oxidative upcycling of catalysts for lab-grade PE/PP mixture was evaluated using an autoclave reactor equipped with a mechanical stirring system (KEMN Instruments, $CHEM^N$: MSG50-P5-T3-SS1-SV-R-ET, Figure S1). In a typical experiment, 100 mg of powdered polymer (comprising 50 wt.% PE and 50 wt.% PP) was physically mixed with 50 mg of MnO_2 and 15 mL of deionized water. The mixture was then transferred into the reactor. Prior to heating, the reactor was sealed and subjected to three cycles of evacuation and pressurization with high-purity air (O_2/N_2, O_2 21 vol%), and then pressurized to 1.5 MPa. The reaction was conducted at 160 °C for 2 h under continuous stirring at 300 rpm, with a heating rate of 5 °C min^{-1}. Upon completion of the reaction, the reactor was allowed to cool naturally. Subsequently, analytical test methods were employed to determine the corresponding products.

Control experiments

In order to investigate the impact of the reaction atmosphere, the experiment was conducted under a nitrogen (N_2) atmosphere instead of using air, employing the standard procedure for catalytic oxidative upcycling of lab-grade PE/PP. To study the importance of catalyst, the same processes were conducted using MnO_2 or without catalysts.

Cycling experiment

To evaluate the reusability of the catalyst, a cycling experiment was devised. Following the aforementioned catalytic oxidative upcycling of PE and PP for 2 h, the reaction was carried out. Subsequently, the catalyst was recovered at the conclusion of each reaction cycle and subjected to drying at 60 °C. The retrieved catalysts from each cycle were then directly employed to initiate subsequent rounds of catalytic oxidative upgrading of PE and PP. Each cycle involved the utilization of 50 mg of catalyst, 50 mg of PE, and 50 mg of PP. The cycling process was repeated sequentially for a total of five cycles.

Catalytic oxidative upcycling of lab-grade PE/PP mixture at 4-g scale

A scale-up reaction was performed using a high-pressure stainless steel batch reactor (KEMN Instruments, CHEM^N: MSG1000-P3-T3-SS1-SV-R). A mixture of 4.0 g of lab-grade PE/PP mixture and 1.0 g of β-MnO_2 (Feedstock-to-catalyst weight ratio of 4) was added to 330 mL of deionized water and transferred directly into the reactor. The system was sealed and pressurized to 1.5 MPa with compressed air. The reaction was conducted at 160 °C for 2 h under continuous stirring at 300 rpm. After cooling to room temperature, the mixture was collected. Post-reaction workup and product analysis were carried out as previously described.

Catalytic oxidative upcycling of PE/PP waste plastics

Similar methodologies were applied to pipettes, packaging bags, straws, and plastic lids in accordance with the previously described protocol for catalytic oxidative upcycling of lab-grade PE/PP. The reaction duration was kept constant at 2 h. Prior to the reaction, the mentioned waste plastics were cut into fragments.

Product analysis

Following the completion of the reaction, the system undergoes natural cooling to reach room temperature. The gaseous byproducts are collected using FEP (Teflon) gas bags. Subsequently, a mixture of ethanol (EtOH) is employed for the extraction of both liquid and solid components within the reactor. After sonication for 10 min, all mixtures are subjected to filtration to separate the liquid and solid phases. The liquid fraction is concentrated under reduced pressure to obtain the oil product, while the filtered solid is dried at 60 °C for 24 h prior to collection.

Residual solids analysis:

The solid masses were weighed using a PR124ZH analytical balance (minimum, 0.1 mg). Surface species on the catalysts post-reaction were investigated through

thermogravimetric analysis (TG, NETZSCH TG 209F3) at a temperature ramp rate of 10 °C/min under an air atmosphere. The surface morphology of the used catalyst was examined via TEM (FEI Tecnai G2 F20, Thermo Fisher), and the carbon content distribution on the catalyst surface was analyzed using a HIR944 carbon sulfur analyzer.

Liquid-phase product analysis:

The conversion was further assessed using the carbon-mole conversion (C-Mole conversion), which quantifies the transfer of carbon from the feedstock to oil products during the thermal catalytic oxi-upcycling process. The C-Mole in the product oil and the initial polymer PE were obtained from an elemental analyzer (Elementar VARIO EL11). The Mn content in the liquid products was determined by ICP-OES (Thermo Fisher iCAP PRO). Samples were diluted as needed, and calibration curves were constructed using standard solutions. Measurements were performed in triplicate to ensure accuracy. Oxidation products in the solution were further identified by gas chromatography-mass spectrometry (GC-MS, Agilent 5977B GC/MSD). The GC-MS conditions were as follows: column temperature, 40 °C; injector temperature, 300 °C; split ratio, 5:1; solvent delay, 2.00 min; scan range, m/z 25-500; scan interval, 0.50 s; total scan time, 2.80-32.00 min. Prior to analysis, the degradation products were esterified by adding 10.00 mL of the product solution to 5.00 mL of 50 wt.% BF_3-MeOH solution, followed by heating at 70 °C for 1 h. The reaction was quenched with 2.00 mL of water, and the mixture was extracted multiple times with 5.00 mL of n-hexane and diluted to a final volume of 10.00 mL. Prior to esterification, defined amounts of dicarboxylic acid standards (C_4–C_{22}) were dissolved in methanol and diluted to a final volume of 50.00 mL to prepare a series of gradient standard solutions. These standard solutions were used to construct calibration curves for GC–MS quantitative analysis, based on which the concentrations of the products were determined.

Due to the substantial introduction of oxygen during the reaction, accurately determining the yield is challenging. To overcome this, we employed a straightforward approach by monitoring the mass ratio of oil to feedstock polyolefin throughout the reaction process.

$$Oil/Feedstock\ polyolefin(wt\%) = \frac{Mass_{oil}}{Mass_{feedstock}} \times 100\% \quad (1)$$

Where $Mass_{oil}$ is the mass of the product oil, and $Mass_{feedstock}$ is the mass of initial polymer. The conversion of the substrate PE is calculated as

$$Conversion = \frac{PE\ (imput) - PE\ (residue)}{PE\ (imput)} \times 100\% \quad (2)$$

Where PE (imput) represents the mass of the initial PE input and PE (residue) represents the mass of the residual solid PE material at the end of the reaction. The C-Mole conversion was determined using the following equation

$$C - Mole\ yield = \frac{C - Mole_{oil}}{C - Mole_{feedstock}} \times 100\% \quad (3)$$

Where $Carbon\ Mole_{oil}$ is the mole carbon element in the product oil, and $Carbon\ Mole_{feedstock}$ is the mole of carbon element in the initial polymer.

Gas product analysis:

Gas-phase products were analyzed using a time-of-flight mass spectrometer (TOFMS; SPIMS-3000, Hosin) equipped with an online volatile organic compound (VOC) detector. The acquired data were processed using the SPIMS-3000 VOC data analysis software. In addition, gas chromatography (GC) was performed using an Agilent 7890B system (Agilent Technologies, USA) to characterize the composition of gaseous products. The GC system was equipped with a thermal conductivity detector (TCD) and a flame ionization detector (FID), with helium (99.99%) used as the carrier gas. Two columns were employed: a carbon molecular sieve packed column (3 m, 80–100 mesh) for the separation of permanent gases such as CO_2 and CO, and a HP-PLOT Al_2O_3 capillary column (50 m × 530 μm × 15 μm) for hydrocarbon analysis. A gas sample volume of 250 μL was injected for each run.

Carboxylic acid titration experiment

To ascertain the carboxylic acid concentration within the product oil, we conducted an acid-base titration.[1] Initially, 50 mg of the oil sample obtained after 24 h of reaction underwent precise weighing and subsequent dissolution in ethanol (CO_2-free). A commercially available standard titrant solution of 0.05 mol/L KOH-ethanol was then diluted to 0.01 mol/L with ethanol (CO_2-free) for titration. The titration process was carried out using a fully automated potentiometric titrator (809 Titrando) to ensure accuracy and reliability. The acid value, defined as the amount of potassium hydroxide (KOH) in milligrams required to neutralize the free fatty acids present in one gram of sample, was calculated using the following equation

$$Acid\ value\ (mg\ KOH/g) = \frac{V \times C \times M_{KOH}}{m} \quad (S4)$$

Where V is the volume (in mL) of the KOH solution consumed during titration, C is the molar concentration of the KOH solution (mol/L), M_{KOH} is the molar mass of KOH (56.1 g/mol), and m is the mass of the sample (in g). This formula assumes a complete and stoichiometric neutralization reaction between KOH and the free fatty acids.

Theory calculations

To gain mechanistic insight into the cleavage of internal C–C bonds in PE and the subsequent oxidation of hydrocarbons to carboxylic acids, we first aimed to rationalize the key elementary steps involved in this transformation. As a model catalyst, bulk MnO_2 was first optimized to its antiferromagnetic ground state to accurately describe its electronic structure. Based on this, a slab model of the thermodynamically most

stable (110) surface was constructed, which exposes four-coordinated (Mn_4) and five-coordinated (Mn_5) Mn sites. Among them, the Mn_4 site was identified as the preferred active site for dissociative adsorption of molecular O_2, thereby generating reactive surface oxygen species essential for initiating and propagating the oxidation steps.

The β-MnO_2 primitive unit cell in the tetragonal phase was first fully optimized using the structure downloaded from the Materials Project website (mp-510408). The optimized lattice vectors of a = b = 4.430 Å and c = 2.874 Å. The most stable (110) surface of MnO_2 tetragonal phase was simulated by a 5×3×1 supercell slab model including three MnO_2 sub-layers (90 Mn atoms and 180 O atoms, totally) separated by a vacuum layer with a thickness of 15 Å along the surface normal direction to avoid spurious interactions between periodic slab models. The bottom two layers of MnO_2 were fixed, while the rest was allowed to relax during the geometry optimization. The lattice parameters were fixed throughout the surface calculations. The Brillouin zone integration and k-point sampling were restricted to the gamma point. The nudged-elastic band method with the improved tangent estimate (CI-NEB) was used to determine the minimum energy path and to locate the transition state structure for each elementary reaction step.[2] Transition state was confirmed by observing only one imaginary frequency corresponding to each reaction coordinate. The adsorption energy of the reaction intermediate was calculated as $E_{ads} = E_{adsorbate+surface} - E_{adsorbate} - E_{clean-surface}$. The activation energy (E_a) of a chemical reaction was defined as the energy difference between the initial and transition states, while the reaction energy (ΔE) was defined as the energy difference between the initial and final states. Geometries were visualized by VESTA.[3]

Preparation of modified PVA film

Modified PVA films were prepared via a solution-casting method. Specifically, 10 wt.% of PVA powder was dispersed in deionized water and stirred at 80 °C until completely dissolved to obtain the PVA casting solution. For the modified films, a mixed acid product accounting for 5 wt.% relative to the PVA powder was obtained from the oxidative degradation of PE/PP at 160 °C under 1.5 MPa of air for 2 h using MnO_2 as the catalyst. This acid mixture was dissolved in 1 mL of anhydrous ethanol and subsequently added to the PVA casting solution. The mixture was stirred at 65 °C for 2 h to ensure homogeneity. After standing for 30 min to remove bubbles, the solution was cast onto a polyvinylidene fluoride (PVDF) mold and dried at room temperature for 48 h to obtain the target PVA film samples.

Film characterization

Thicknesses for the films were tested by electronic thickness gage (ProGage 40\100, Thwing-Albert, US). The mechanical properties of the obtained films were performed on universal tensile testing machine (INSTRON5493, USA). All the samples were divided into rectangles at 5 × 20 mm following by using the stretching rate at 0.2 mm/min. The film transmittance was measured using a U3900 ultraviolet–visible (UV–Vis) spectrophotometer (Hitachi, Tokyo, Japan) at 200-800 nm. Optical properties, including the transmittance value (T) and haze (H) of the films, were measured with a

WGT/S haze and transmittance testing machine (Shanghai Precision Instrument Co., Shanghai, China). Water contact angles were performed using optics-based contact angle measuring equipment (Attension Theta Flex, Sweden). The thermostability was studied by a thermogravimetric analysis instrument (NETZSCH STA 409PC, Germany) in nitrogen gas flow at 10 °C/min.

Antibacterial activity of the developed films was evaluated using two bacterial strains: *E. coli* ATCC 25922 and *S. aureus* ATCC 6538. The assay was conducted with modifications based on the method reported by Chen et al.[4] Film samples (0.4 g) were sterilized under UV light for 30 min and then transferred into test tubes containing 10 mL of tryptic soy broth (TSB). A total of 100 μL of bacterial suspension at the exponential growth phase (approximately 10^5 CFU/mL) was inoculated into the tubes containing the film samples. The cultures were incubated at 37 °C by shaking at 200 rpm for 12 h. After incubation, the bacterial suspensions were serially diluted and plated onto tryptic soy agar (TSA) plates. The plates were then incubated at 37 °C for 24 h, after which the number of colonies was counted.

II. Supplementary Figures

Figure S1. Autoclave reactor equipped with a mechanical stirring system for the catalytic oxidative upcycling of PE/PP mixture (KEMN Instruments, CHEM^{N}: MSG50-P5-T3-SS1-SV-R-ET).

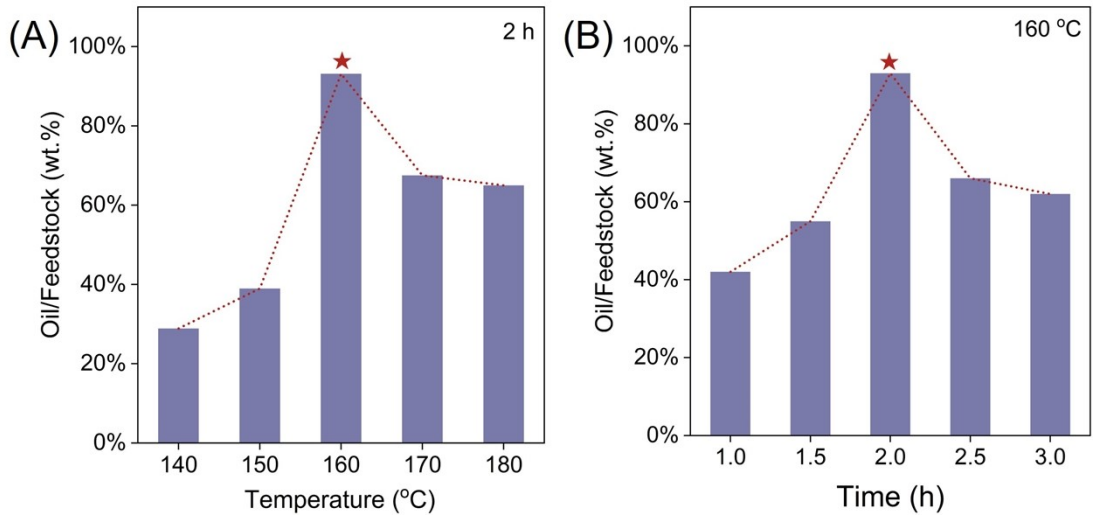

Figure S2. Catalytic oxidative upcycling of PE/PP mixture under different temperatures and reaction durations. Reaction conditions: 50 mg β-MnO_2, 50 mg PE pellets (M_w, 4.0×10^3 g mol^{-1}), 50 mg PP pellets (M_w, 1.2×10^4 g mol^{-1}), 15 mL H_2O, 1.5 MPa air, 140-180 °C, 1-3 h, magnetic stirring 300 rpm.

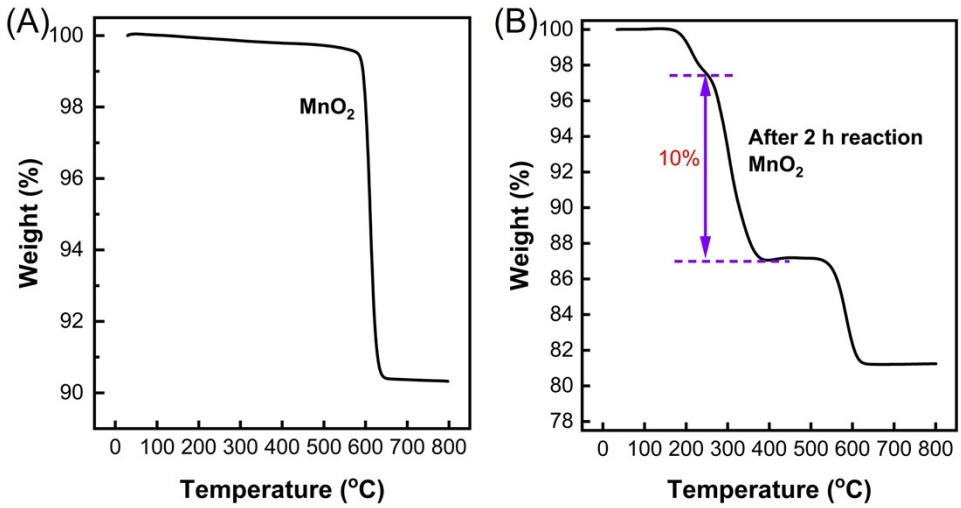

Figure S3. TG profiles of β-MnO_2 catalyst before and after the reaction.

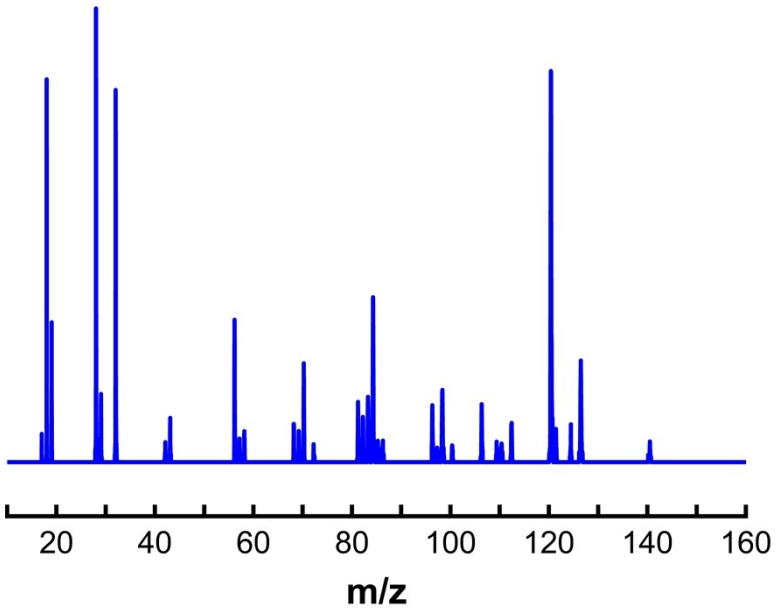

Figure S4. TOFMS profile for gaseous volatiles from the catalytic disassembly of PE/PP mixture after reaction.

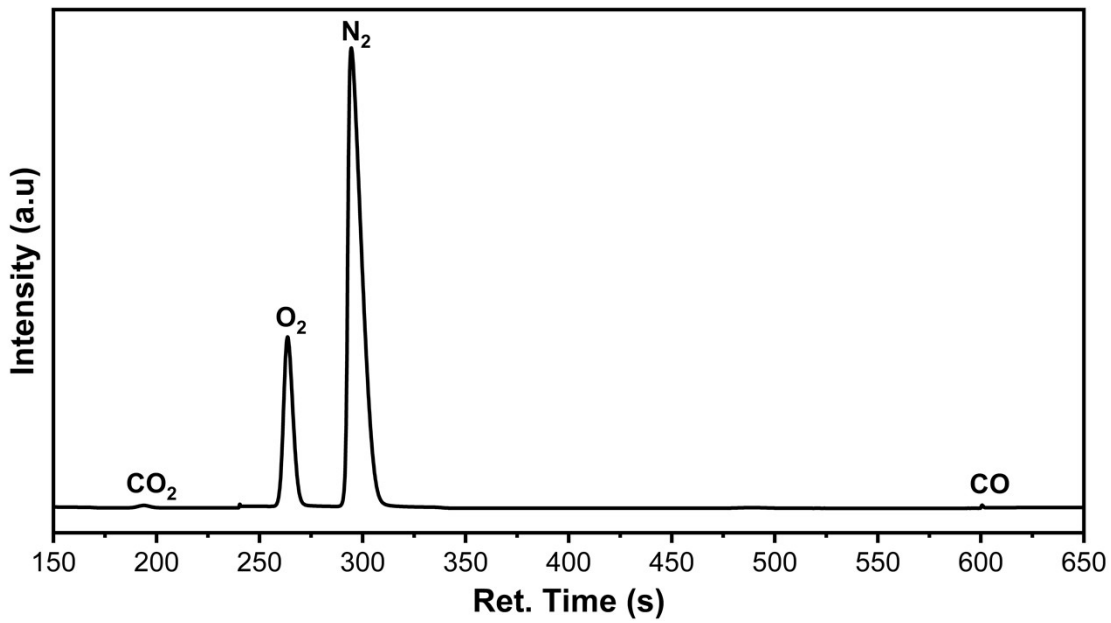

Figure S5. GC-TCD analysis of the gas products obtained from PE/PP mixture oxidative upcycling using β-MnO_2.

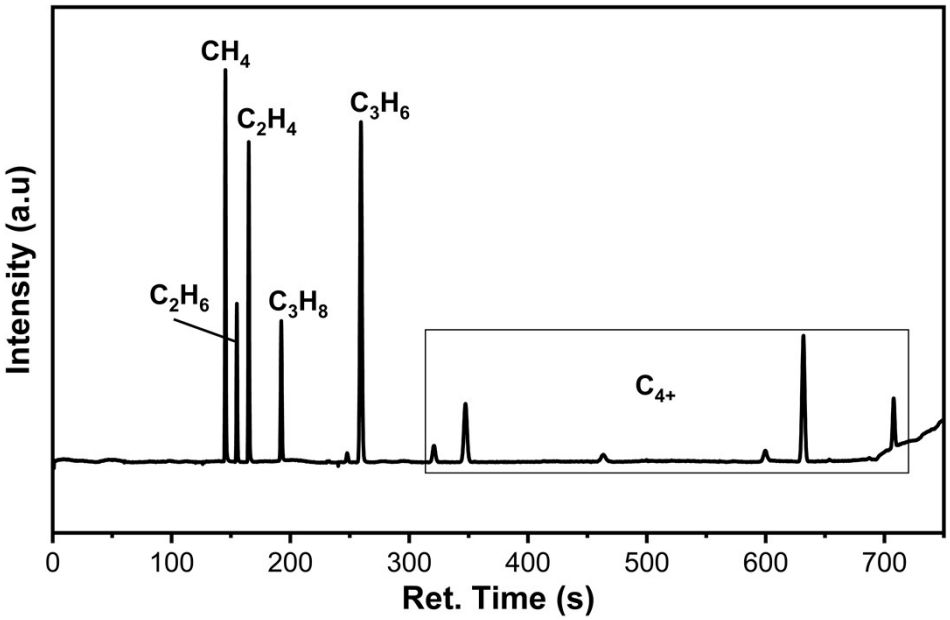

Figure S6. GC-FID analysis of the gas products obtained from PE/PP mixture oxidative upcycling using β-MnO_2.

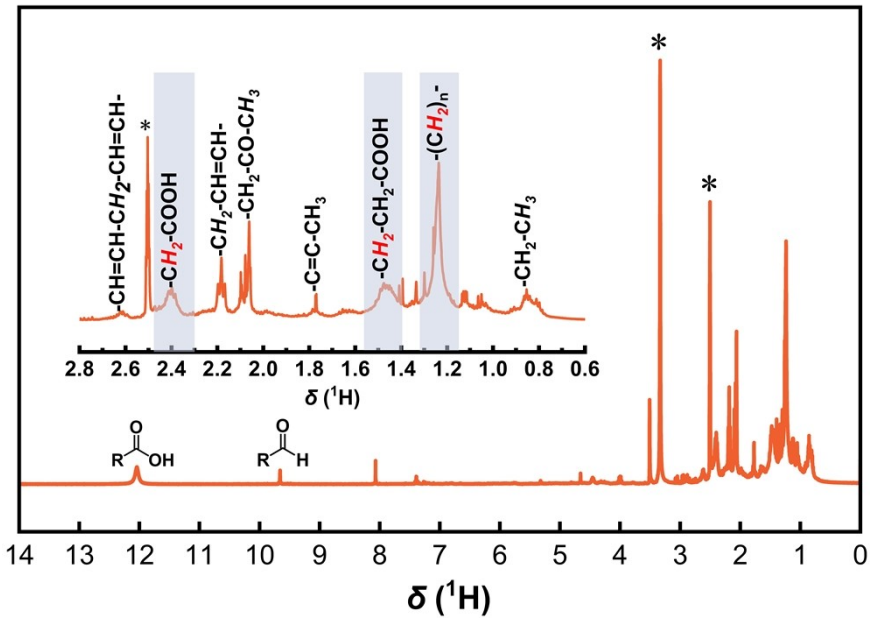

Figure S7. ^{1}H NMR spectrum of the produced oil from the catalytic oxidative upcycling of PE/PP mixture after 2 h of reaction. * Indicates the water and solvent peaks (DMSO-d*6*).

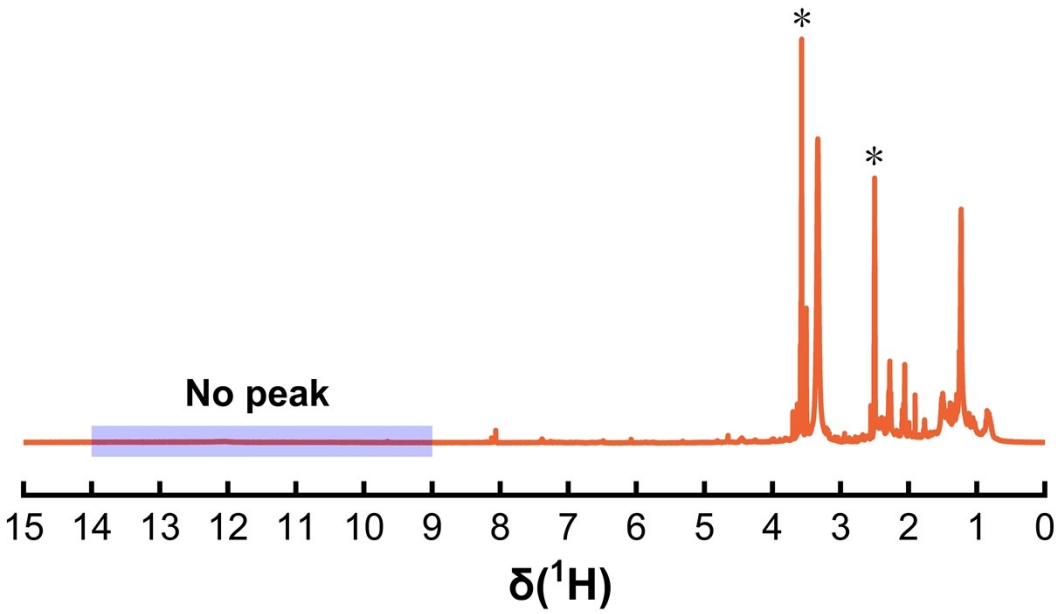

Figure S8. ^{1}H NMR spectrum of the oil (2 h of reaction) after methyl esterification. * Indicates the water and solvent peaks (DMSO-d*6*). Methyl esterification was carried out using 100 mg of oil, 10 mL of MeOH, and 5 mL of 50 wt.% BF_3–MeOH solution under reflux at 70 °C for 1 h.

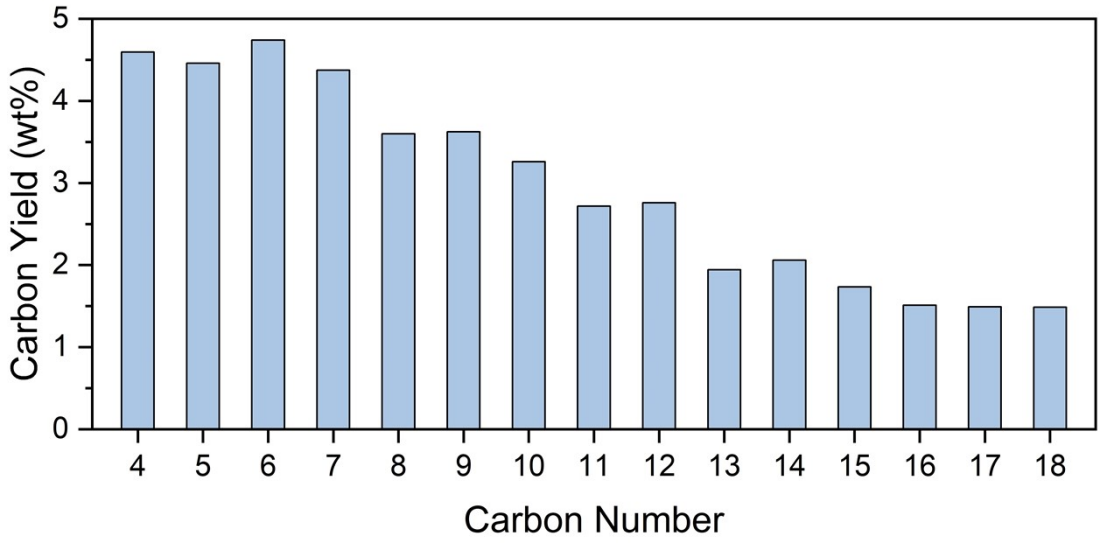

Figure S9. Carbon-number distribution of aliphatic dicarboxylic acids from β-MnO_2-catalyzed oxidation of PE/PP mixtures. Reaction conditions: 50 mg β-MnO_2, 50 mg PE pellets (M_w, 4.0×10^3 g mol^{-1}), 50 mg PP pellets (M_w, 1.2×10^4 g mol^{-1}), 15 mL H_2O, 1.5 MPa air, 160 °C, 2 h, magnetic stirring 300 rpm.

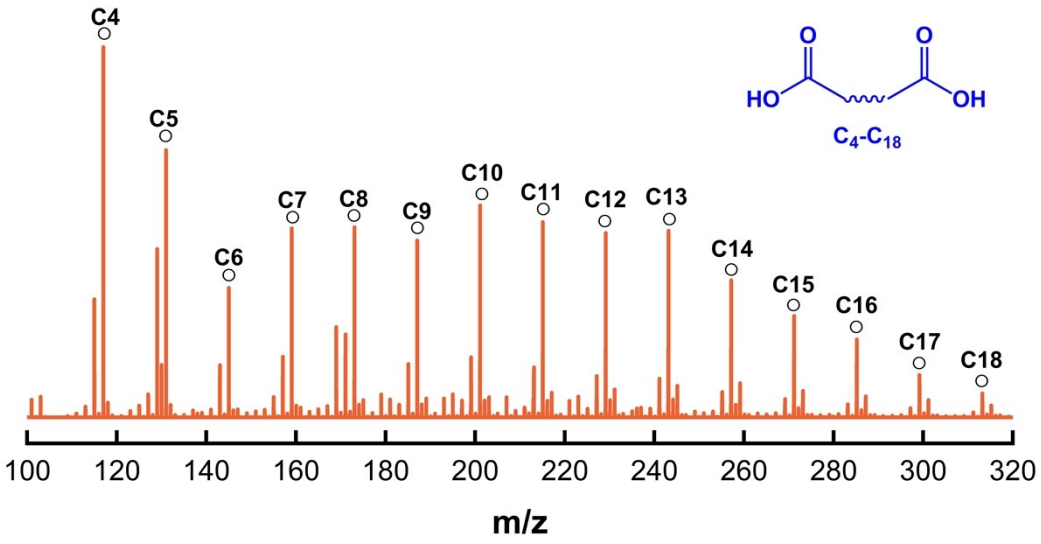

Figure S10. HRMS spectrum of the liquid-phase product. Reaction conditions: 50 mg MnO_2 (or other catalysts), 50 mg PE particles (M_w, 4.0×10^3 g mol^{-1}), 50 mg PP pellets (M_w, 1.2×10^4 g mol^{-1}), 15 mL H_2O, 1.5 MPa air, 160 °C, 2 h, mechanical stirring at 300 rpm.

Figure S11. Photograph of the produced oil of the cyclic reaction dissolved in EtOH.

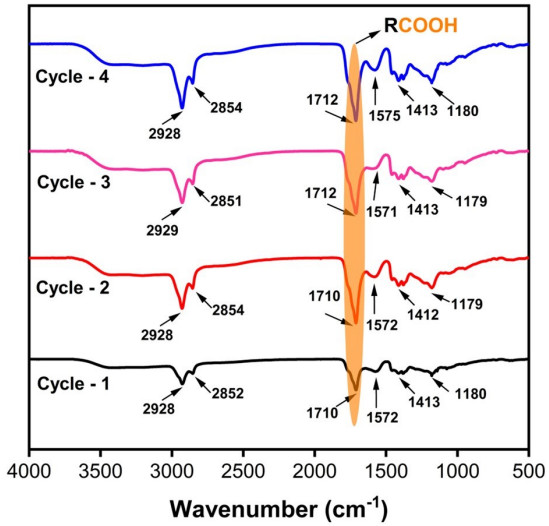

Peak (cm^{-1})	Functional group
1180	C-O stretching vibration
1412	C-O stretching band
1572	C=C stretching vibration
1710	C=O stretching vibration of the carboxylic acid group
2852	C-H stretching (symmetry)
2927	C-H stretching (asymmetry)

Figure S12. FTIR spectra and the peak assignments of the oil from the catalytic oxidative upcycling of PE/PP mixture after cycles of reaction.

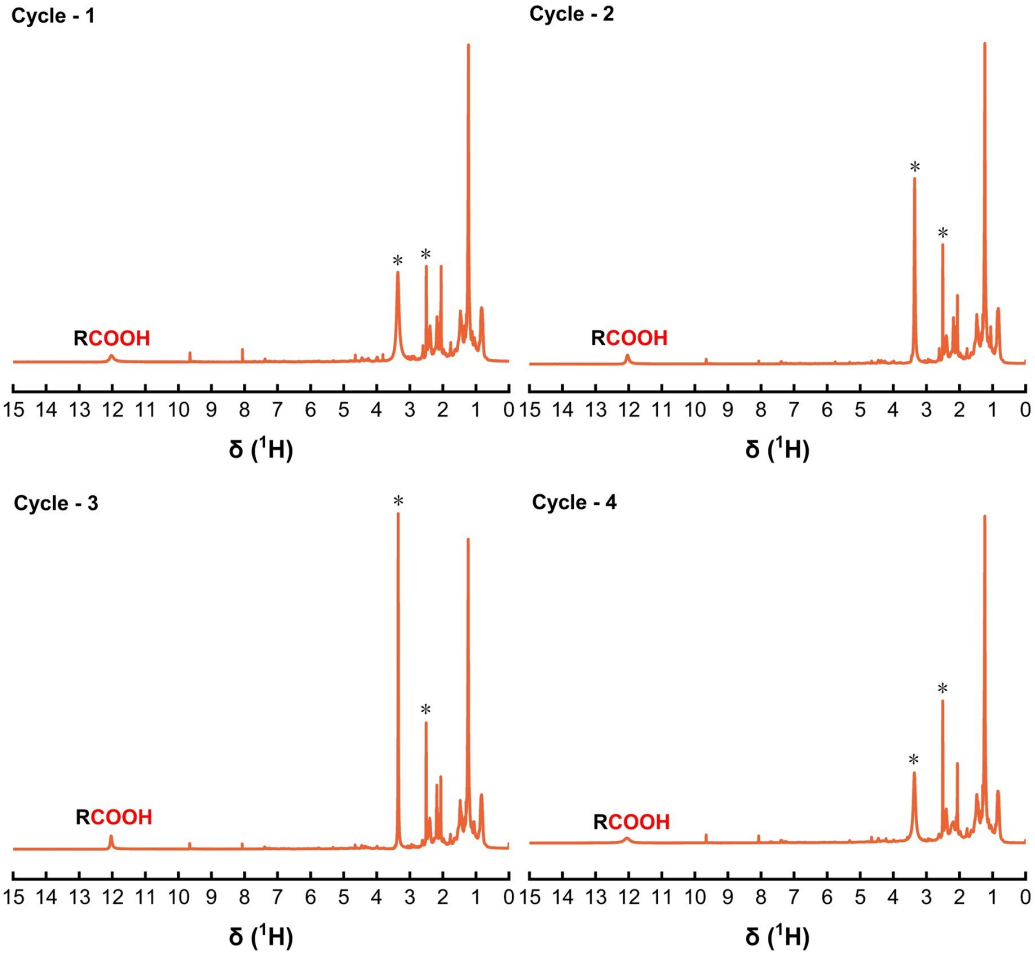

Figure S13. ^{1}H NMR spectra of the product oil from the catalytic oxidative upcycling of PE/PP mixture after cycle of reaction. * Indicates the water and solvent peaks (DMSO-d*6*).

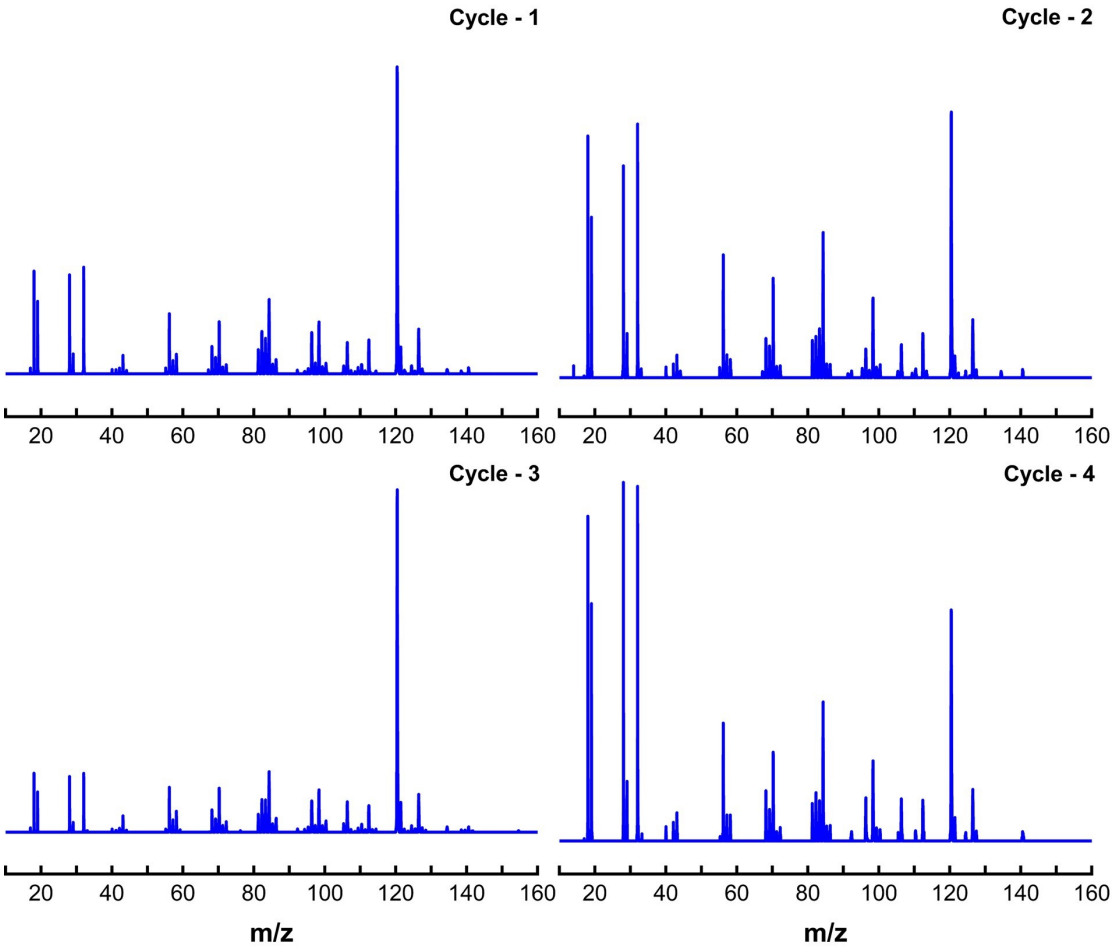

Figure S14. TOFMS profiles of gaseous volatiles from the catalytic oxidative upcycling of PE/PP mixture after cycle of reaction.

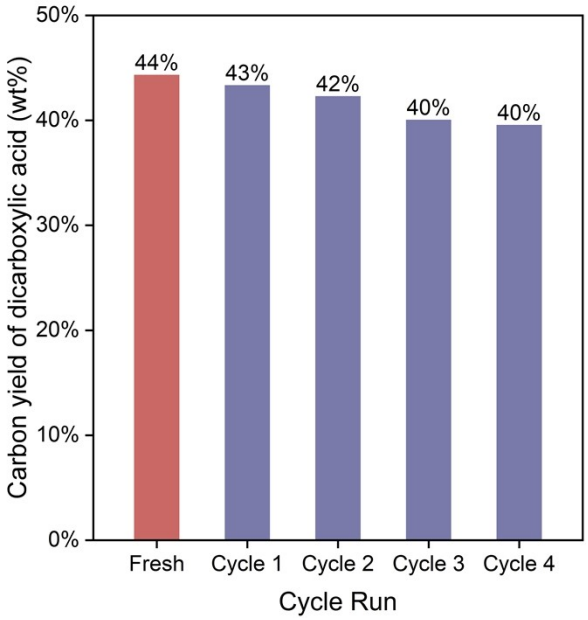

Figure S15. Diacid yield for each catalytic recycling run over MnO_2.

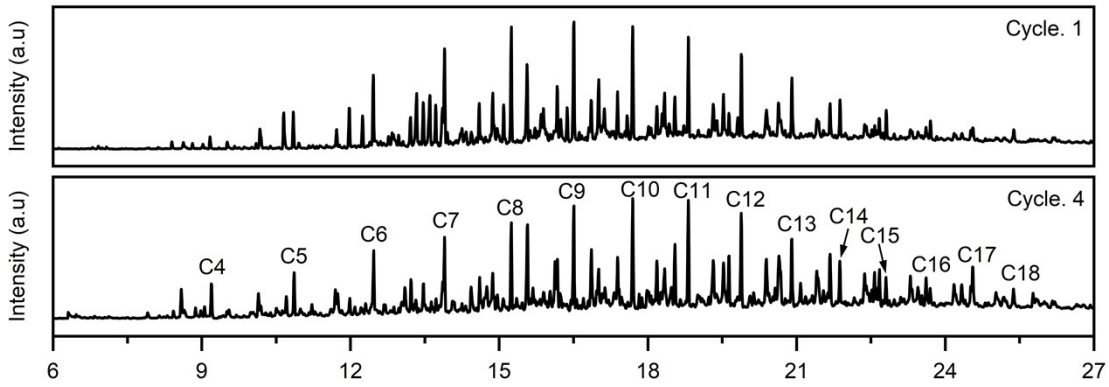

Figure S16. GC–MS chromatograms of products obtained from catalytic oxidative upcycling of a PE/PP mixture after the 1st and 4th reaction cycle.

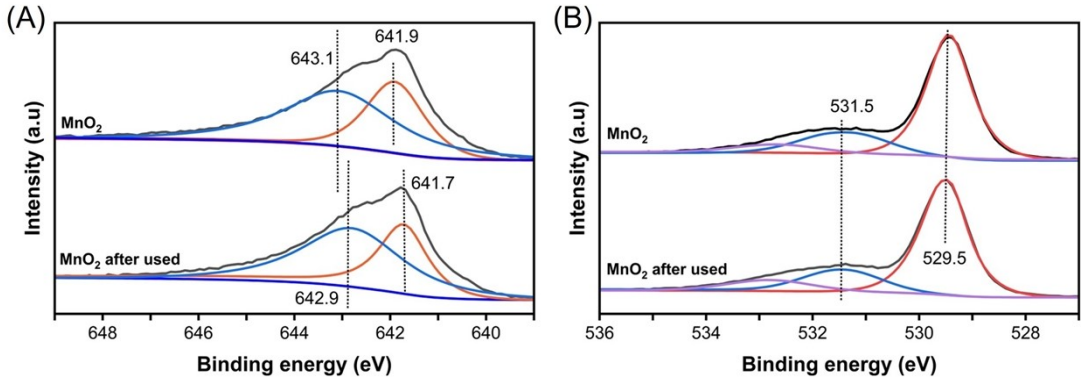

Figure S17. XPS spectra of β-MnO_2 catalysts before and after the reaction. (A) Mn 2*p*; (B) O 1*s*.

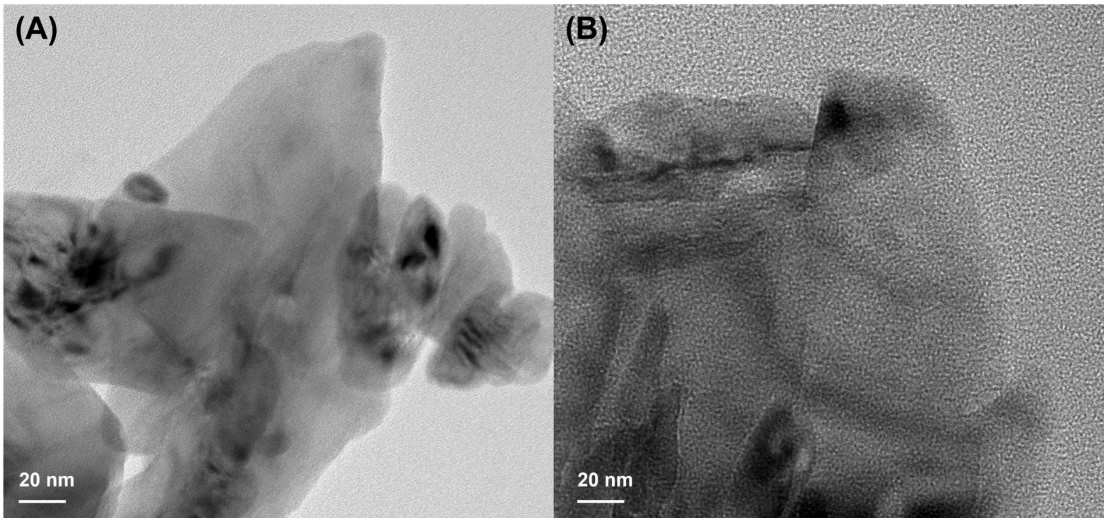

Figure S18. TEM images of MnO_2 catalysts before (A) and after (B) the reaction.

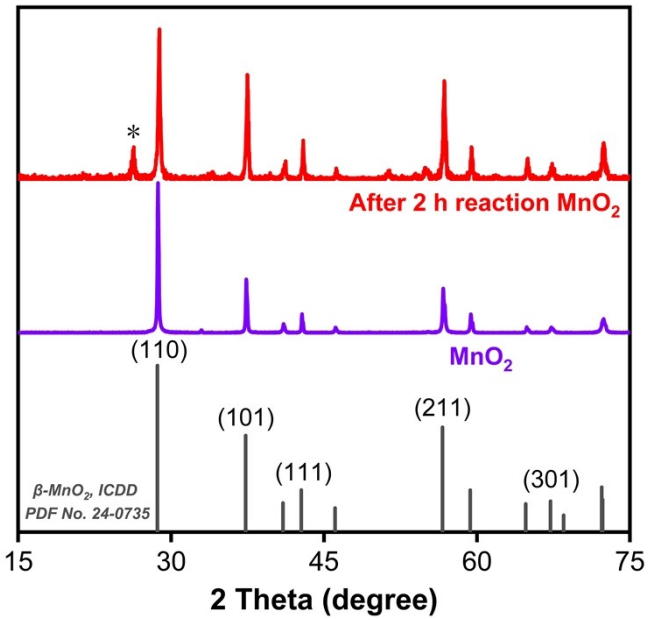

Figure S19. XRD patterns of MnO_2 catalyst before and after the reaction. * Indicates the diffraction peak at around $2\theta \approx 26.4°$, which is commonly assigned to the (002) plane of carbonaceous materials (ICDD PDF No. 75-1621).

Figure S20. Setup of the scale-up catalytic reaction in a high-pressure stainless steel batch reactor (KEMN Instruments, CHEM^{N}: MSG1000-P3-T3-SS1-SV-R).

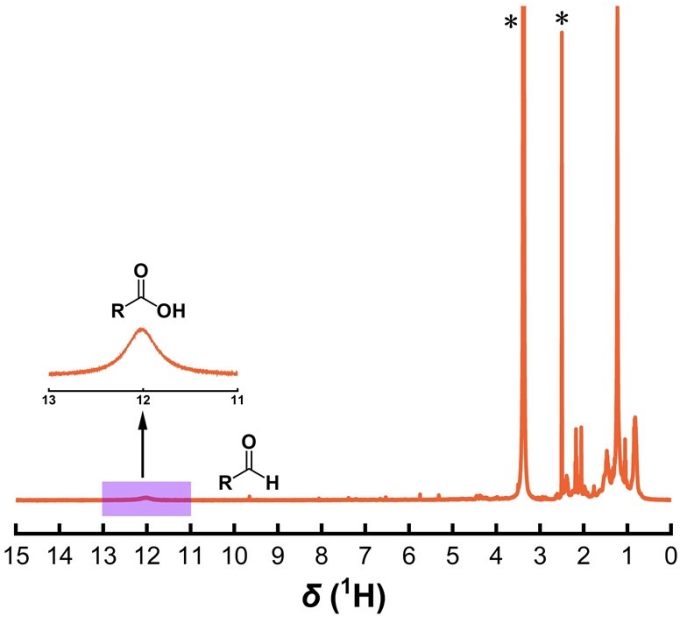

Figure S21. ^{1}H NMR spectrum of the oil product obtained from the scale-up catalytic oxidative upcycling of PE/PP mixture after 2 h of reaction. * Indicates the water and solvent peaks (DMSO-d*6*).

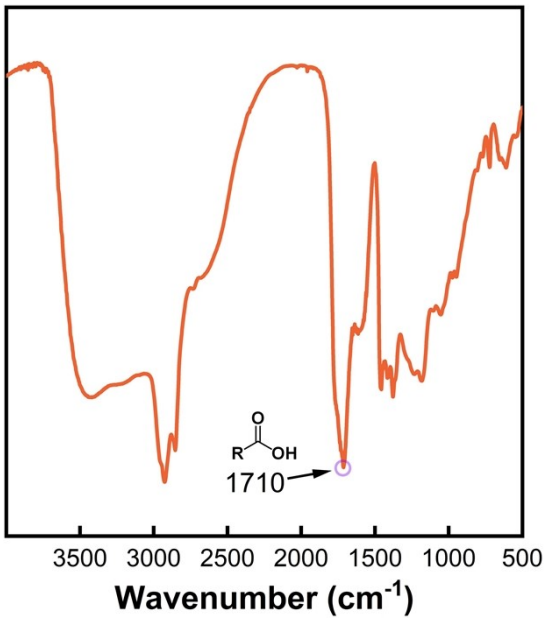

Figure S22. FTIR spectrum of the oil product obtained from the scale-up catalytic oxidative upcycling of PE/PP mixture after 2 h of reaction.

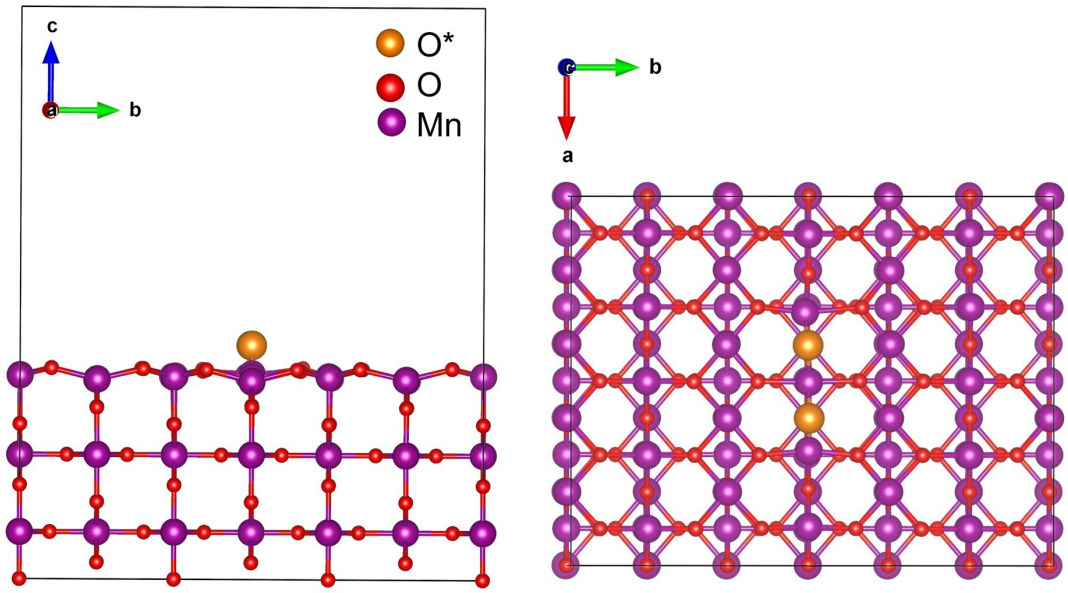

Figure S23. Slab model used in the DFT calculations. Top (left) and side (right) views of the (110) surface of β-MnO_2 with two dissociatively adsorbed oxygen species (O).

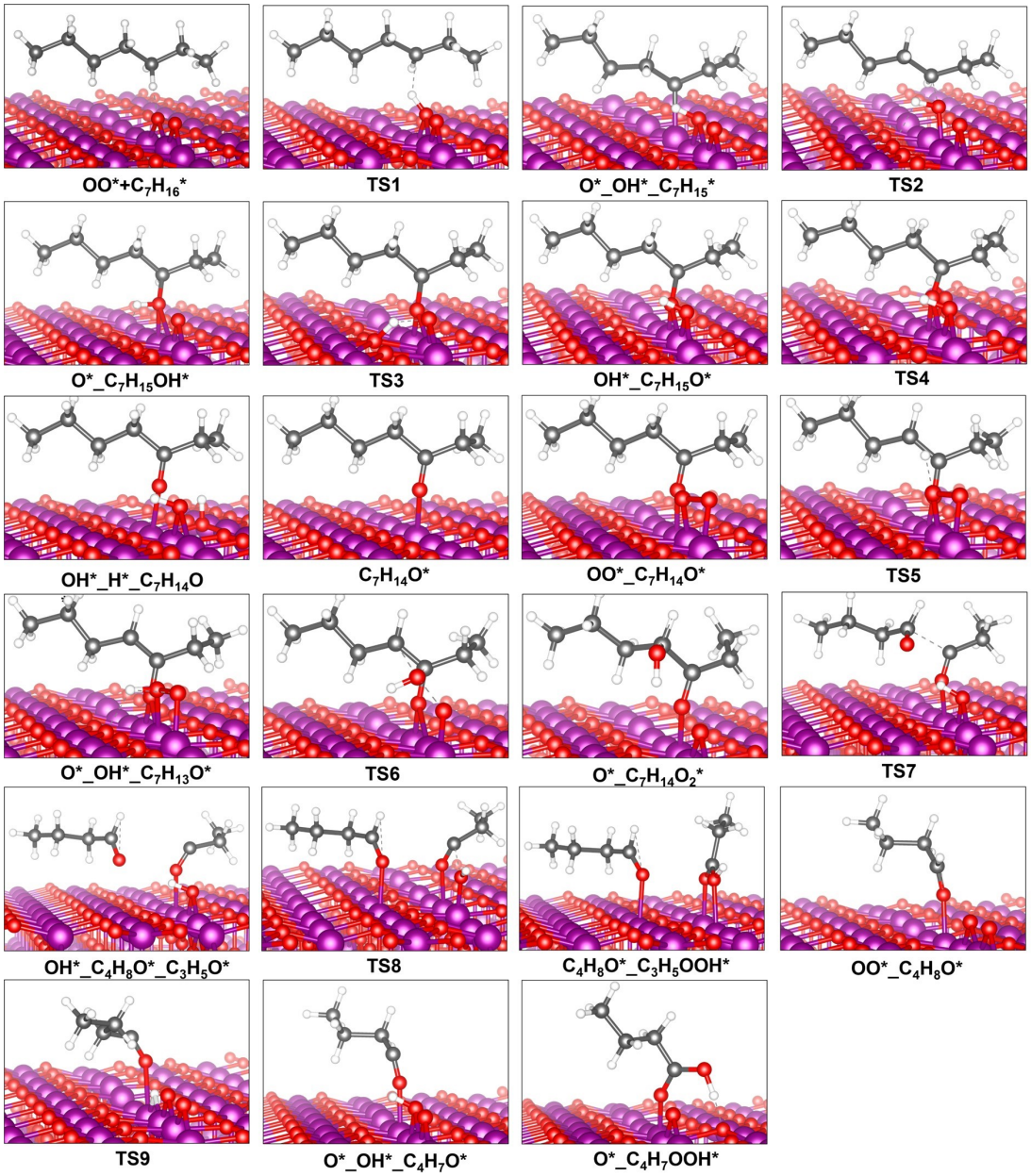

Figure S24. Local geometries of all DFT-optimized reaction intermediates and transition states of oxidative degradation of PE over the (110) surface of β-MnO_2.

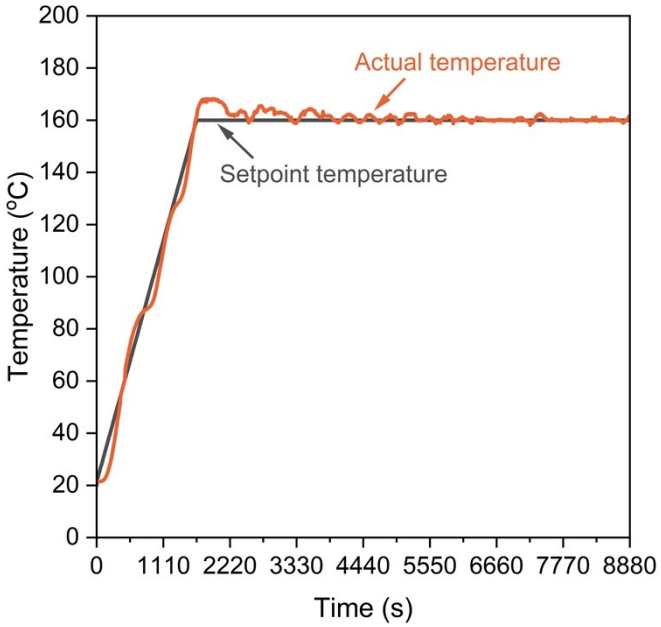

Figure S25. Temperature profile of the reaction system over time.

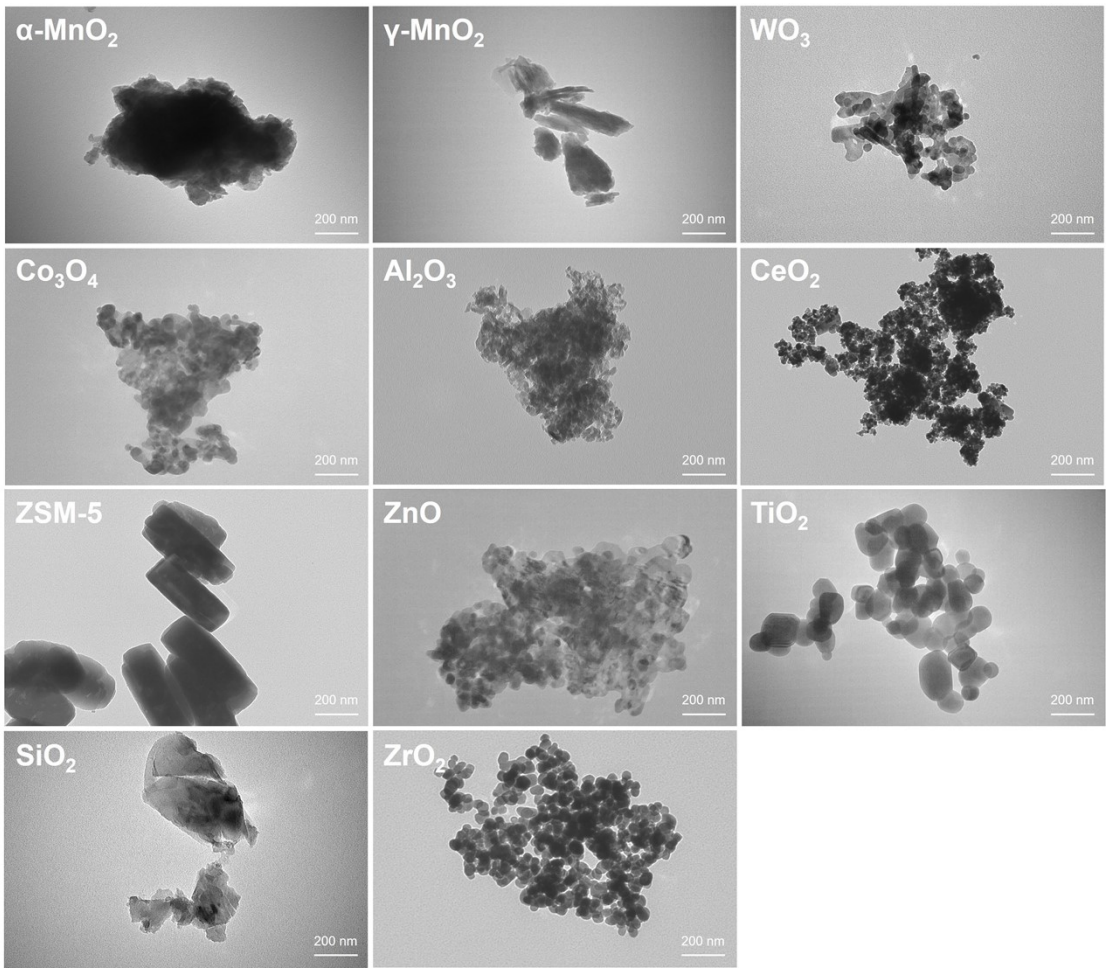

Figure S26. TEM images of different catalysts.

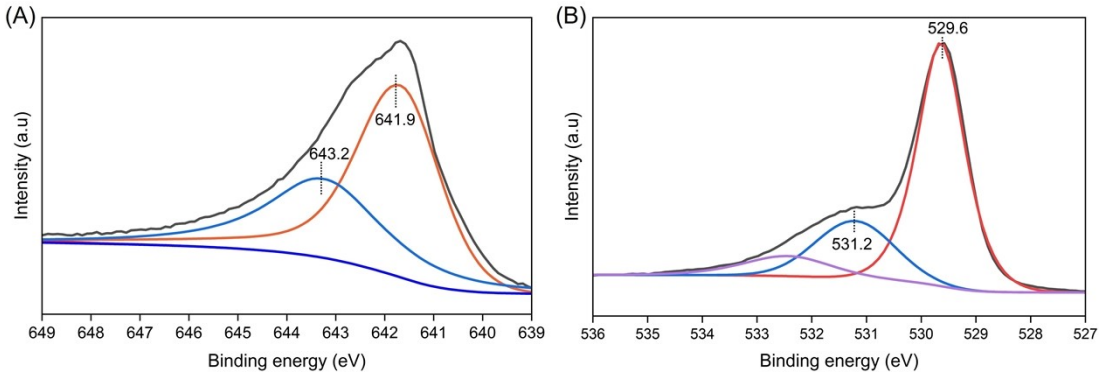

Figure S27. XPS spectra of β-MnO_2 catalysts after ball milling. (A) Mn 2*p*; (B) O 1*s*.

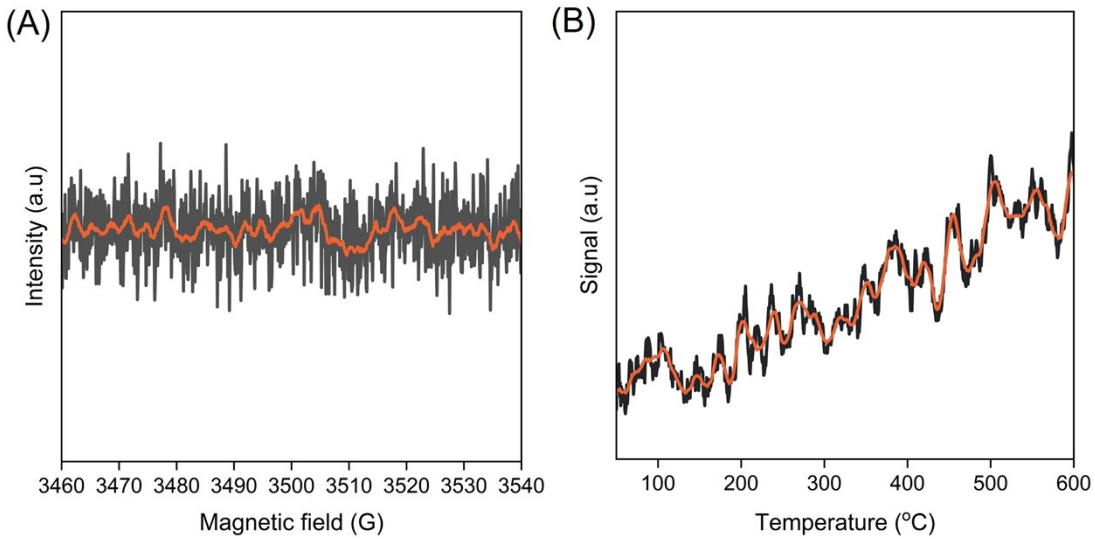

Figure S28. Characterization of oxygen vacancies and surface acidity of β-MnO_2. (A) EPR spectra and (B) NH_3-TPD profiles.

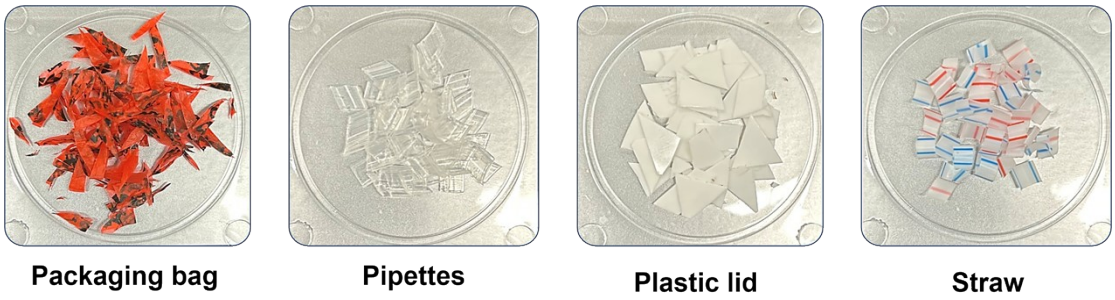

Figure S29. Photograph of waste plastics after cutting up.

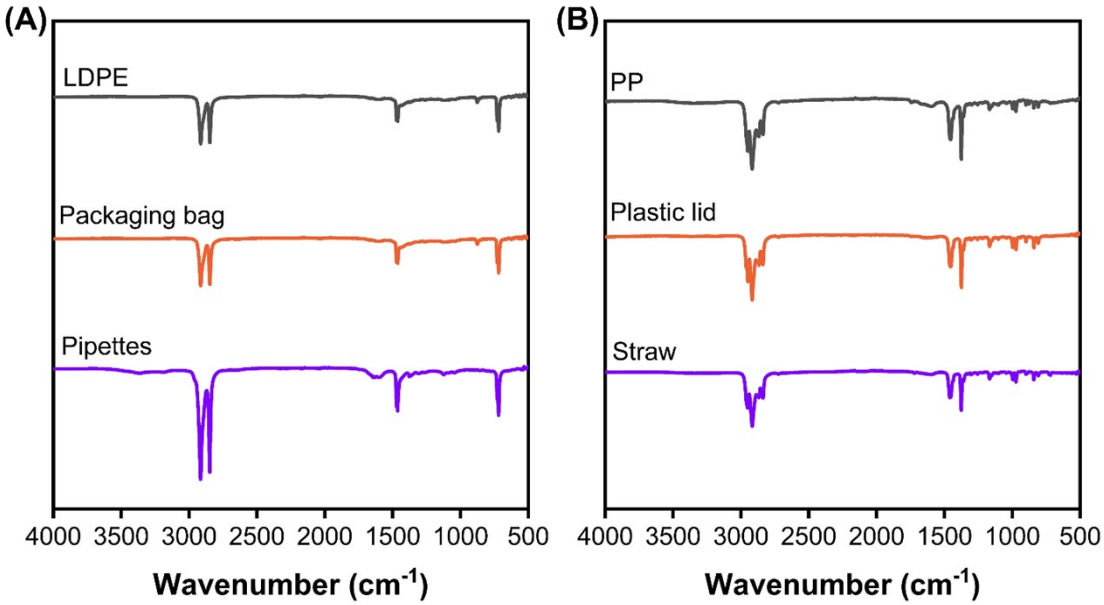

Figure S30. FTIR spectra of various types of PE (A) and PP (B).

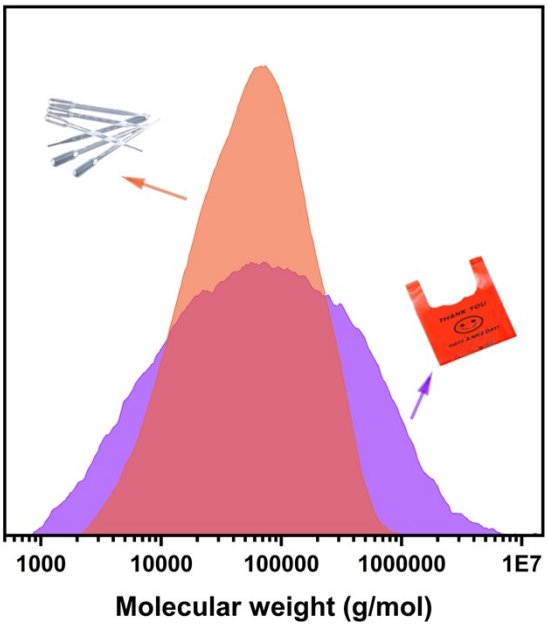

Sample	*Mp* (g mol^{-1})	*Mn* (g mol^{-1})	*Mw* (g mol^{-1})	PD
Pipettes	6.79×10^4	2.85×10^4	9.09×10^4	3.20
Packaging bag	7.16×10^4	1.71×10^4	2.40×10^5	14.04

Figure S31. HT-GPC analysis of pipettes and packaging bag.

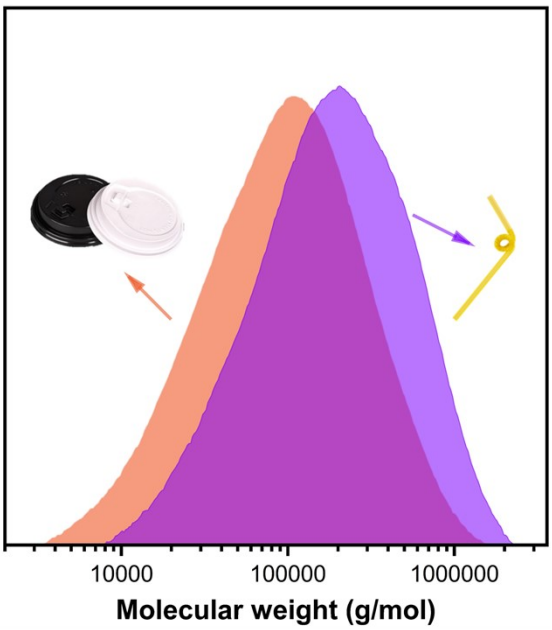

Sample	*Mp* (g mol^{-1})	*Mn* (g mol^{-1})	*Mw* (g mol^{-1})	PD
Plastic lid	1.10×10^5	4.93×10^4	1.54×10^5	3.13
Straw	2.04×10^5	1.03×10^5	2.90×10^5	2.82

Figure S32. HT-GPC analysis of plastic lid and straw.

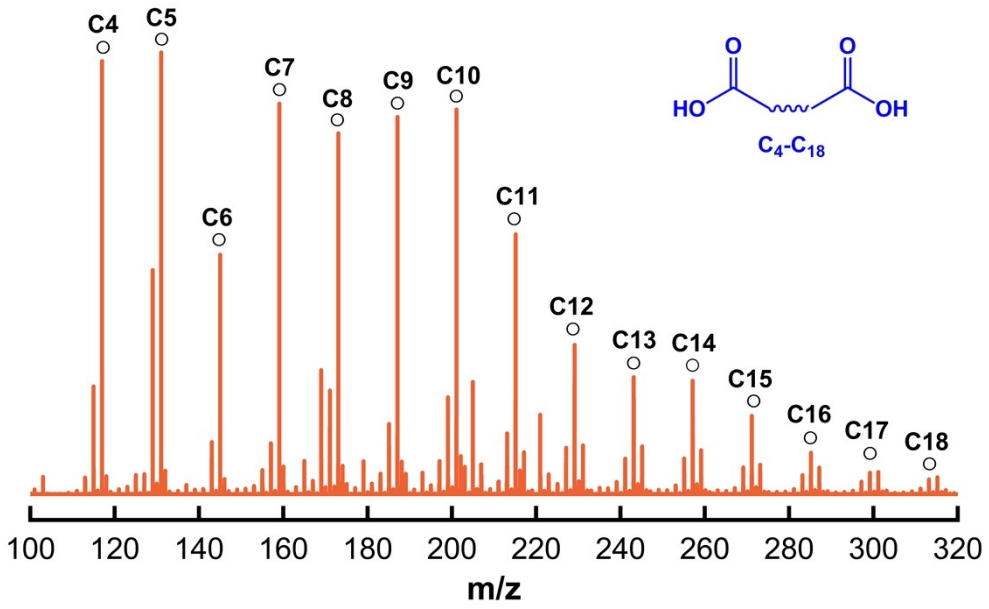

Figure S33. HRMS spectrum of the produced oil from the catalytic oxidative upcycling of PE/PP mixture after 2 h of reaction. Reaction conditions: 50 mg MnO_2, 100 mg mixture (packaging bag (M_w, 2.40×10^5 g/mol), pipettes (M_w, 9.09×10^4 g/mol), plastic lip (M_w, 1.54×10^5 g/mol), straw (M_w, 2.90×10^5 g/mol), each of 25 mg),15 mL H_2O, 1.5 MPa air, 160 °C, 2 h, mechanical stirring 300 rpm.

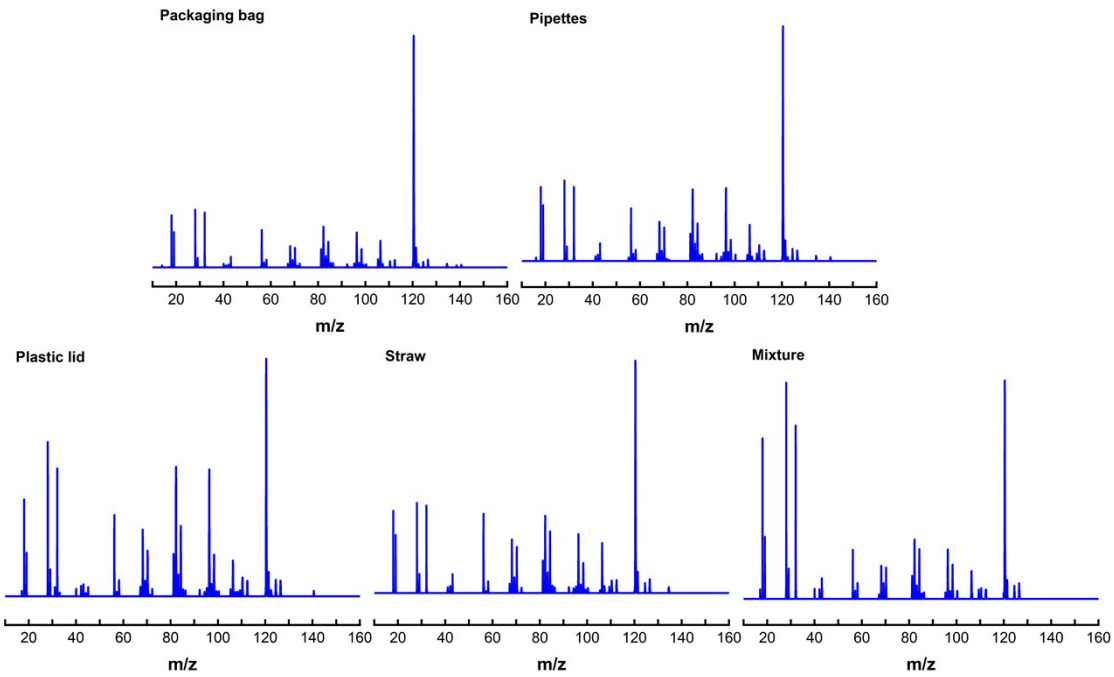

Figure S34. TOFMS profiles of gaseous volatiles from the catalytic oxidative upcycling of different feedstock samples after 2 h of reaction.

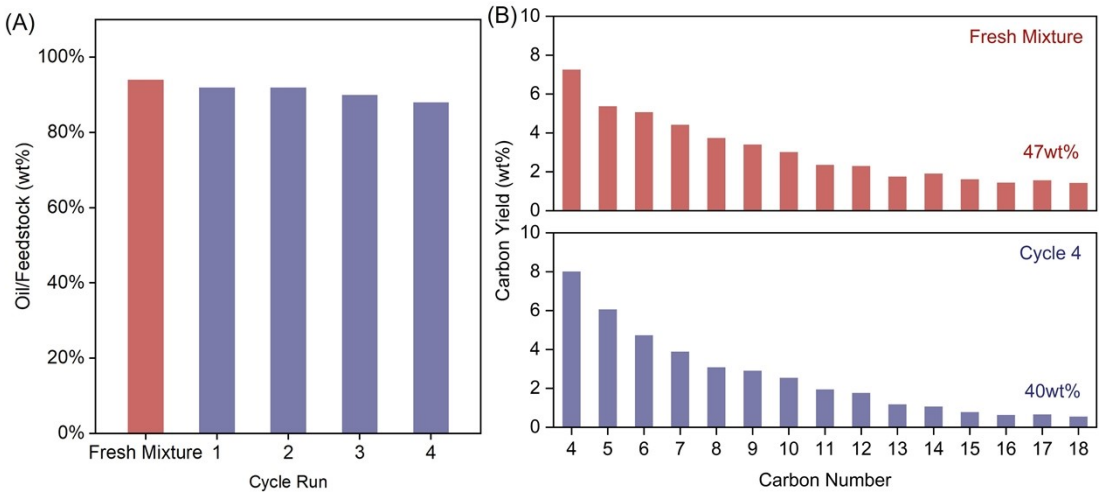

Figure S35. Catalytic recycling performance of MnO_2 using mixed real waste plastics as feedstock. (A) Oil yield during catalytic recycling. (B) Comparison of diacid distribution before reaction and after four catalytic cycles.

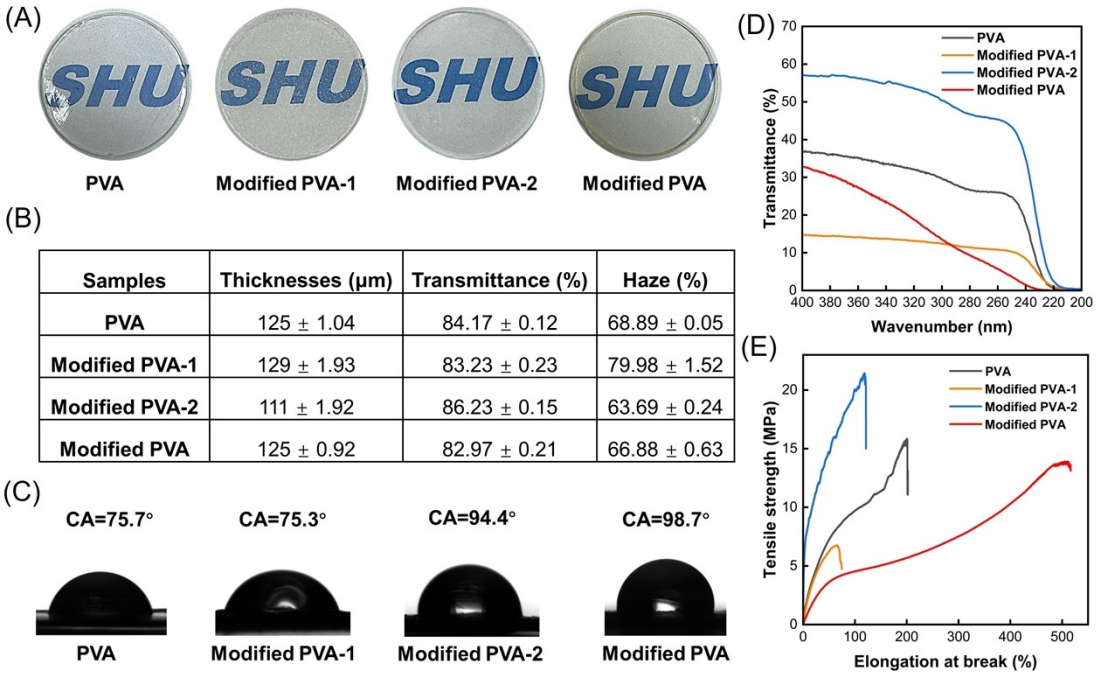

Samples	Thicknesses (μm)	Transmittance (%)	Haze (%)
PVA	125 ± 1.04	84.17 ± 0.12	68.89 ± 0.05
Modified PVA-1	129 ± 1.93	83.23 ± 0.23	79.98 ± 1.52
Modified PVA-2	111 ± 1.92	86.23 ± 0.15	63.69 ± 0.24
Modified PVA	125 ± 0.92	82.97 ± 0.21	66.88 ± 0.63

Figure S36. Characterization of the PVA films incorporating different additives. (A) Photographs of the film, (B) optical performance, (C) water contact angle, (D) UV shielding capacity, and (E) mechanical properties. The films incorporating the oxidized degradation products of PE/PP, decanoic acid, and sebacic acid are labeled as modified PVA, modified PVA-1, and modified PVA-2, respectively.

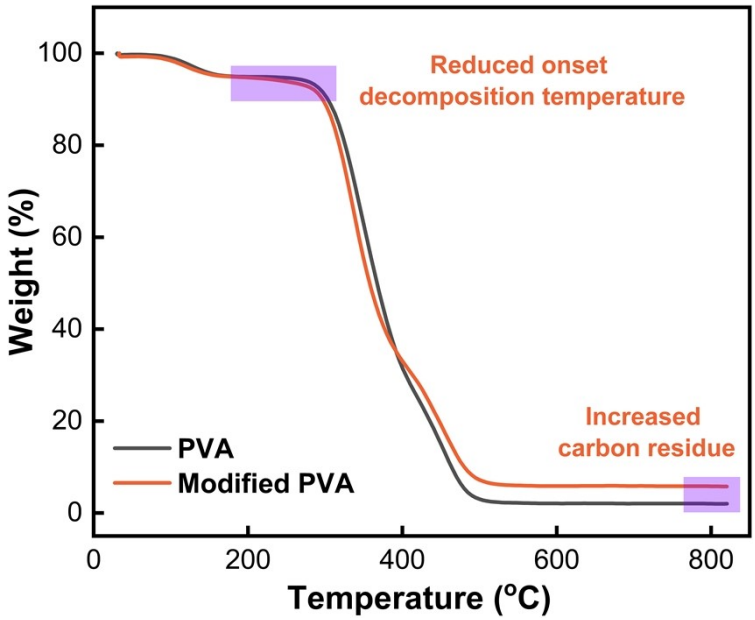

Figure S37. TG profiles of PVA and modified PVA films.

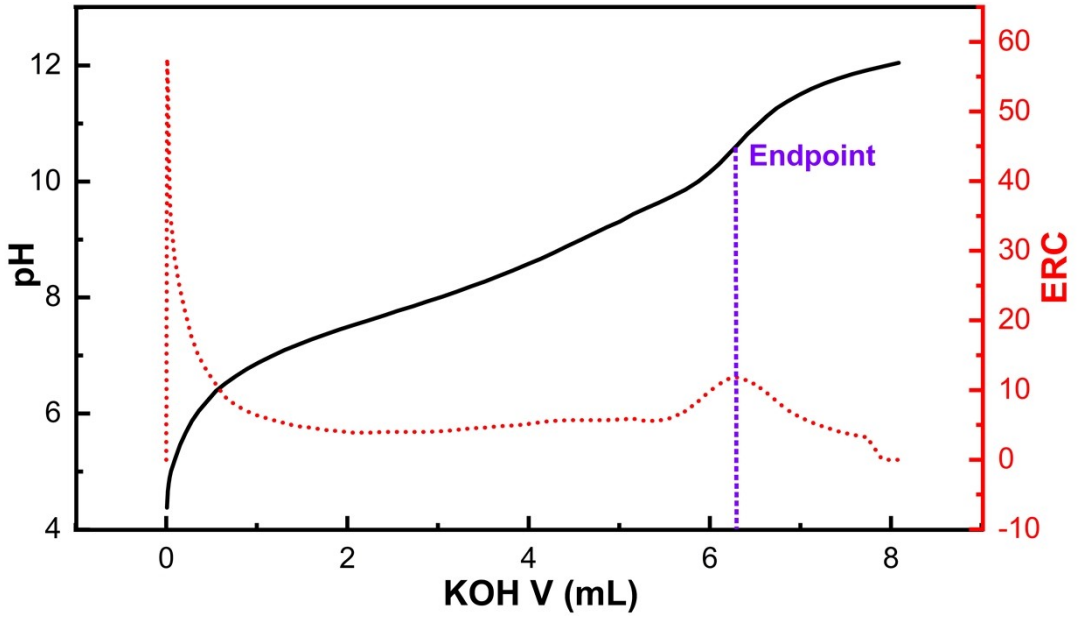

Figure S38. pH titration curve of KOH-ethanol standard titration solution for 2 h product oil-ethanol solution. Titration method: 12 mg (accurately weighed)-ethanol (CO_2 removed) solution, 0.01 mol/L KOH-ethanol standard titration solution with an automatic potentiometric titrator (809 Titrando).

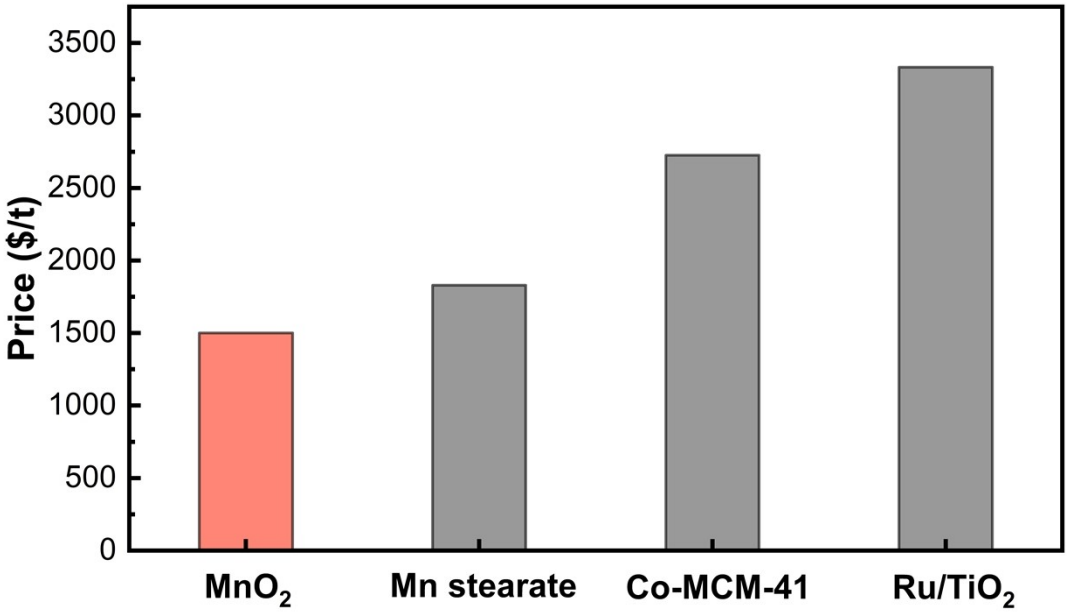

Figure S39. The market price of the catalyst used for the oxidative upcycling of polyolefin plastics. *Cost estimations are based on publicly available market prices from http://www.made-in-china.com, converted from RMB to USD (May 2025).

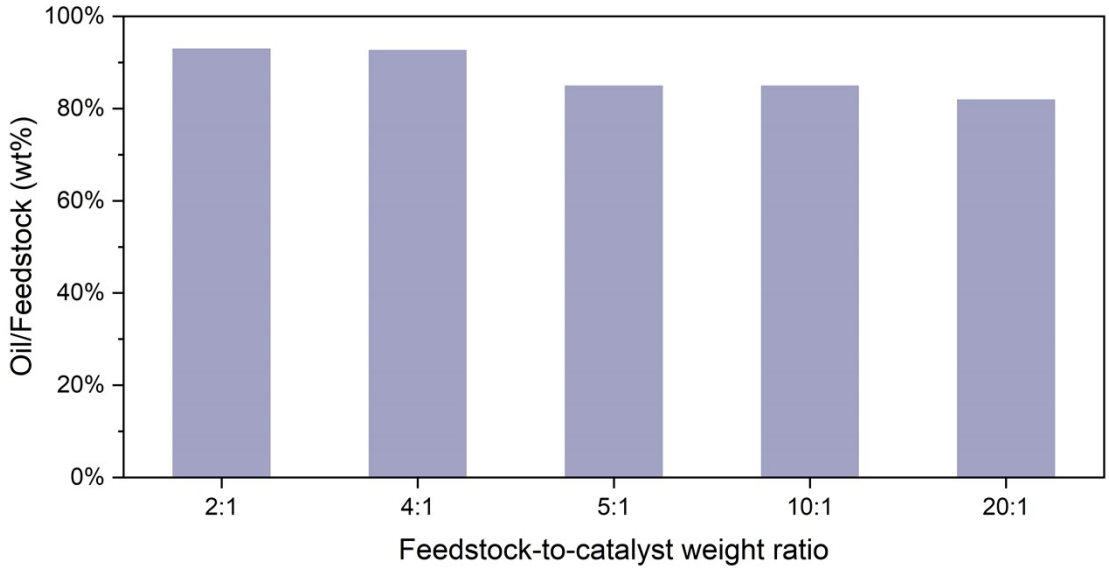

Figure S40. MnO_2-catalyzed oxidative upcycling of PE/PP mixtures at different feedstock-to-catalyst weight ratios.

III. Supplementary Tables

Table S1. The mass ratio of C and H in the following samples (catalyst, β-MnO_2) was detected by elemental analyzer.

Samples	C (wt.%)	H (wt.%)
LDPE (M_w, 4×10^3 g mol^{-1})	85	14
PP (M_w, 1.2×10^4 g mol^{-1})	86	14
Packaging bag (M_w, 1.71×10^4 g mol^{-1})	86	14
Pipettes (M_w, 1.10×10^5 g mol^{-1})	86	13
Straw (M_w, 2.04×10^5 g mol^{-1})	85	14
Plastic lid (M_w, 1.10×10^5 g mol^{-1})	85	14
Fresh, oil	56	8
Cycle. 1, oil	59	9
Cycle. 2, oil	59	8
Cycle. 3, oil	57	8
Cycle. 4, oil	51	7
Packaging bag (M_w, 1.71×10^4 g mol^{-1}), **oil**	54	9
Pipettes (M_w, 2.85×10^4 g mol^{-1}), **oil**	56	8
Plastic lid (M_w, 1.10×10^5 g mol^{-1}), **oil**	51	7
Straw (M_w, 2.04×10^5 g mol^{-1}), **oil**	52	7
Mixture(M_w, 2.40×10^5 g mol^{-1}), **oil**	59	10

Table S2. The mass ratio of C in the following samples (different catalysts) was detected by elemental analyzer.

Samples	**C (wt.%)**
α-MnO_2, Oil	56
γ-MnO_2, Oil	53
WO_3, Oil	50
Co_3O_4, Oil	51
Al_2O_3, Oil	49
CeO_2, Oil	47
ZSM-5, Oil	44
ZnO, Oil	40
TiO_2, Oil	40
SiO_2, Oil	40
ZrO_2, Oil	39

Table S3. Comparison to different works in the oxi-upcycling of PE plastics.

Catalyst	T (°C)	Pressure	Time (h)	Product	Ref.
Mn-stearate[a]	150	50 mL/s air flow	10	Fatty acids	5
Ru/TiO_2	160	1.5MPa air	24	Dicarboxylic	6
Co-MCM-41	125	1.0MPa O_2	12	Long chain diacids	7
TS-1 zeolite[b]	140-200-140	1.5MPa air	12	Dicarboxylic	8
MnO_2	160	1.5MPa air	2	Carboxylic acid mixture	This work

[a] Before the reaction, the feedstock was thermally cracked at 360 °C for 8-16 h.
[b] The gradient-temperature method consists of three stages: stage one at 140 °C for 1 h, stage two at 200 °C for 2 h, and stage three at 140 °C for 9 h.

Table S4. Control experiment conditions and phenomena.

Experiment	Reaction conditions	Oil/Feedstock (wt.%)
1	50 mg MnO_2, 50 mg PE pellets (M_w, 4.0×10^3 g mol^{-1}), 50 mg PP pellets (M_w, 1.2×10^4 g mol^{-1}), 15 mL H_2O, 1.5 MPa air, 160 °C, 2 h, mechanical stirring 300 rpm.	93
2	50 mg MnO_2, 50 mg PE pellets (M_w, 4.0×10^3 g mol^{-1}), 50 mg PP pellets (M_w, 1.2×10^4 g mol^{-1}), 15 mL H_2O, 1.0 MPa O_2, 160 °C, 1 h, mechanical stirring 300 rpm.	91
3	50 mg MnO_2, 50 mg PE pellets (M_w, 4.0×10^3 g mol^{-1}), 50 mg PP pellets (M_w, 1.2×10^4 g mol^{-1}), 15 mL H_2O, 1.5 MPa N_2, 160 °C, 2 h, mechanical stirring 300 rpm.	5
4	$Mn(CH_3COO)_2\cdot4H_2O$ in an amount equimolar to 50 mg of MnO_2, 50 mg PE pellets (M_w, 4.0×10^3 g mol^{-1}), 50 mg PP pellets (M_w, 1.2×10^4 g mol^{-1}), 15 mL H_2O, 1.5 MPa air, 160 °C, 2 h, mechanical stirring 300 rpm.	52
5	50 mg PE pellets (M_w, 4.0×10^3 g mol^{-1}), 50 mg PP pellets (M_w, 1.2×10^4 g mol^{-1}), 15 mL H_2O, 1.5 MPa air, 160 °C, 2 h, mechanical stirring 300 rpm.	39

Table S5. The specific surface area (BET) of different catalyst.

Sample	BET (m^2/g)
α-MnO_2	27.6
γ-MnO_2	30.0
WO_3	0.6
Co_3O_4	3.5
Al_2O_3	141.6
CeO_2	41.5
ZSM-5	406.2
ZnO	27.8
TiO_2	11.8
SiO_2	0.6
ZrO_2	31.0

Table S6. The specific surface area (BET), pore volume, and pore size of MnO_2 samples.

Sample	BET (m^2/g)	Pore Volume (cm^3/g)	Pore Size (nm)
β-MnO_2	3.3	0.005	18.04
β-MnO_2 after ball milling	9.6	0.057	31.10

Table S7. ICP-OES analysis of Mn content in Liquid Products

Sample* quality (mg)	Test element	Element content of sample (%)
93	Mn	5.34

*Reaction conditions: 50 mg β-MnO_2, 50 mg PE pellets (M_w, 4.0×10^3 g mol^{-1}), 50 mg PP pellets (M_w, 1.2×10^4 g mol^{-1}), 15 mL H_2O, 1.5 MPa air, 160 °C, 2 h, mechanical stirring 300 rpm.

IV. References

[1] S. Mahajan, S. K. Konar, D. G. B. Boocock, *J. Am. Oil Chem. Soc.*, 2006, **83**, 567-570.

[2] G. Henkelman, B. P. Uberuaga, H. Jónsson, *J. Chem. Phys.*, 2000, **113**, 9901-9904.

[3] K. Momma, F. Izumi, *J. Appl. Crystallogr.*, 2011, **44**, 1272-1276.

[4] J. Chen, Y. Li, Y. Wang, S. Yakubu, H. Tang, L. Li, *Food Packag. Shelf Life*, 2022, **33**, 100915.

[5] Z. Xu, N. E. Munyaneza, Q. Zhang, M. Sun, C. Posada, P. Venturo, N. A. Rorrer, J. Miscall, B. G. Sumpter, G. Liu, *Science*, 2023, **381**, 666-671.

[6] K. Wang, R. Jia, P. Cheng, L. Shi, X. Wang, L. Huang, *Angew. Chem. Int. Ed.*, 2023, **62**, e202301340.

[7] Q. Zhang, J. He, X. Wei, C. Shen, P. Ye, W. An, X. Liu, H. Li, S. Xu, Z. Su, Y. Wang, *Angew. Chem. Int. Ed.*, 2024, **63**, e20240751.

[8] X. Hou, F. Yuan, X. Liu, K. Wang, Y. Zhu, P. Cheng, R. Jia, L. Shi, L. Huang, *Chem. Eng. J.*, 2005, **504**, 158868.